Friction
https://doi.org/10.1007/s40544-024-0863-x
ISSN 2223-7690
CN 10-1237/TH
RESEARCH ARTICLE

Topology optimization of AISI 4140 steel with surface texture filled by multi-solid lubricants for enhancing tribological properties

Qipeng HUANG[1,2], **Chaohua WU**[1,*], **Xiaoliang SHI**[1,*], **Kaipeng ZHANG**[1]

[1] *School of Mechanical and Electronic Engineering, Wuhan University of Technology, Wuhan 430070, China*

[2] *School of Transportation and Logistics Engineering, Wuhan University of Technology, Wuhan 430063, China*

Received: 03 July 2023 / Revised: 22 September 2023 / Accepted: 18 December 2023

Abstract: Wind power gears will be excessively worn due to lubrication failure during operation. Herein, the tribological properties of rubbing pairs are improved by filling solid lubricants into surface texture. In texture design, three types of topological textures (Circle (C), Hexagon (H) and Circle/Hexagon (CH)) were obtained by cell topology optimization, and then three cases with 20%, 30%, and 40% density were designed for each texture. Next, SnAgCu and TiC were deposited in texture of AISI 4140 steel (AS) to obtain 9 kinds of self-lubricating surfaces. Among them, AS with 30% CH density (AS-CH30) exhibits excellent mechanical and tribological properties. Compared with AS-C and AS-H, the maximum equivalent stress of AS-CH was decreased by 10.86% and 5.37%, respectively. Friction coefficient and wear rate of AS-CH30 were 79.68% and 78% lower than those of AS. The excellent tribological performances of AS-CH30 can be attributed to the synergistic effect of topological surface and solid lubricants. Topological surface can not only reduce fluctuation of equivalent stress, but also promote the stored lubricants to be easily transferred at the contact interface to form a 200 nm lubricating film containing solid lubricants (mainly), oxides and wear debris.

Keywords: topological texture; nano-TiC; self-lubricating; solid lubrication

1 Introduction

As the core component of wind turbine, gearbox often fails, which comes from the lubrication failure and excessive wear of gear (material: AISI 4140 steel (AS)) [1, 2]. Therefore, improving the mechanical and tribological properties and stability of gear tribo-pair (AS/AS) is one of the key issues to promote service performance of wind power gears. In the methods of improving tribological properties of materials, adding lubricating medium (oil/grease), material and/or component design, or using advanced surface engineering are often used [3, 4]. Among these technologies, surface texture technology and solid lubricant coating are the two most promising methods to decrease friction and wear under different requirements (such as heavy load, long life, complex environment, superlubricity, etc.) [5–8].

Surface texture technology is to prepare microstructure arrays with specific shapes, arrangements, and sizes on the surface to obtain specific properties. Initially, the conventional textures of regular geometry were mainly studied, mainly including circle [9], groove [10], ellipse [8], triangle, quadrilateral, hexagon, diamond, and channel [6, 11, 12]. Subsequently, some body surfaces with high wear-resistant (shells and snake skins, etc.) and specific functions (tree frog toes and fish epidermis, etc.) have received the increasing attention [7]. A series of bionic textures have been designed and discovered, such as wavy [13], fanned [14], hexagonal [15], and crescent-shaped [7, 16]. This bionic texture will be simplified or neglected

* Corresponding author: Chaohua WU, E-mail: wuchaohua@whut.edu.cn; Xiaoliang SHI, E-mail: sxl@whut.edu.cn

to some extent. Therefore, the parameters and shapes of bionic texture need to be optimized to achieve excellent performance [17]. Topology optimization can determine the optimal structure, which has been widely used in engineering field of macroscopic structures (such as negative Poisson's ratio, zero or negative thermal expansion coefficient, extreme thermal conductivity, etc. [18, 19]). Grejtak et al. [20] first applied topology optimization to reduce wear loss in tribology, and then Jia et al. [21] used topology surface to decrease friction temperature rise. Compared with the materials with the same volume fraction, the average temperature rise of composites with topological structure were reduced by 40%–60%. Therefore, topology optimization used into bionic texture design of tribology is expected to improve the mechanical and tribological properties of AS.

Solid lubricants play a crucial role in the tribological properties of composites [6, 22]. Researchers have conducted a lot of explorations from the types of lubricants and additives [23, 24]. On the one hand, a variety of lubricants were mixed into multi-lubricants (WC/DLC/WS_2, YSZ/Au/MoS_2/DLC, YSZ/Ag/Mo-TiN, and SnAgCu, etc. [15, 25, 26]) to achieve different functions. On the other hand, tribological properties of materials were also enhanced by introducing additives (two-dimensional layered materials [27], MXenes [8, 28], and nanomaterials [29], etc.). Zhao et al. [30] introduced the MoS_2/$MoSe_2$ into bionic honeycomb topology. Compared with pure Al_2O_3, average coefficient of friction (COF) of the composite was reduced by more than 30%. Our research team found that nano-TiC and SnAgCu as multi-solid lubricants have good adsorption properties with AS, which is conducive to the formation of a stable tribo-film [15, 31]. Therefore, the multi-solid lubricants of nano-TiC and SnAgCu are filled into the topological texture, which is expected to significantly improve the tribological properties of AS.

The synergistic effect of surface texture and solid lubricants can regulate friction and wear [6, 8]. Lu et al. [32] reported the self-lubricating materials prepared by depositing PEO/PTFE coatings in circular texture. At 5 N, the material can effectively reduce COF. Wang et al. [33] prepared a hexagonal texture on the surface of alloy and deposited PTFE. The composite coating exhibited stable low COF (less than 0.2) and zero wear performance under the conditions of atmospheric, deionized water, seawater, and corrosive acidic media. In addition, Liu et al. [34] deposited the fluorinated graphene-MoS_2 nanocomposite coating on the surface of stainless steel with dimple texture. The average COF was reduced to 0.036. Vladescu et al. [35] used the synergistic effect of concentrated polymer brushes and textures to reduce the COF of bearing steel to 0.0006. Therefore, this paper improves the tribological properties of AS by surface topological texture combined with solid lubricants.

In previous researches, we studied the bionic hexagonal texture [17], modified solid lubricants [15, 31] and synergistic effects of surface texture and solid lubricants [36], respectively. However, the solid lubricants filled in the texture will be excessively consumed at the boundary of matrix and solid lubricants during the friction process, which cannot meet the requirements of mechanical properties and self-lubricating properties of AS. Hereby, the bionic texture was further improved by topology optimization in the paper. Effects of topological surface and multi-solid lubricants on the mechanical and tribological properties of AS were studied in dry friction. Morphologies and compositions of worn surfaces and cross-sections were analyzed to reveal the regulation mechanism at the friction interface. This research work could enrich the theory of solid lubrication and guide the design of surface texture, which has important reference value for expanding the application of high-end equipment of self-lubricating materials.

2 Design of topological surface

For improving regulation behavior of surface texture on the tribological properties of self-lubricating materials, bioinspired textures were optimized by cell topology optimization. The optimized cells were arranged periodically to obtain the topological surface.

2.1 Determination of cell structure

In nature, many organisms have evolved unique functional surfaces with mechanically adaptive compatibility to adapt to dynamic changes in interfacial

friction/lubrication. In these surfaces, hexagons exist uniquely in natural biological structures (such as highly abrasive tortoise shells and snake scales, highlyadhesive tree frog toes (Fig. 1), and compound eye structures for panoramic observations [37, 38]) and non-biological structures (such as honeycombs, bubbles, rafts, and snowflakes [39, 40]). Through the exploration of hexagonal structures, it is found that hexagons were not only shape of the most economical material when filling a plane (minimum circumference), but also mechanically stable structure. Therefore, the cell structure is set to hexagon in this study.

2.2 Topology optimization of texture

The bionic topological surface is composed of matrix and solid lubricants. For making the components play the best performance and overall structure meet the engineering requirements, reasonable layout of two materials is an effective design method to achieve the excellent comprehensive performance. The macroscopic properties of topological surface depend on configuration of microstructure. In the design of microstructure, the unit cell texture of AS was designed as a hexagon (Fig. 2(a)).

On the premise of keeping macroscopic material unchanged, the unit cell structure at microscopic scale was topologically optimized. Topology optimization of texture was carried out by Ansys Workbench 19.0. The detailed process consisted of two stages: the first step was to perform static mechanical analysis, and the other step was to perform topology optimization. The specific simulation processes were shown in Fig. 2(b). The whole simulation unit includes counterpart ball (upper) and AS specimen (lower). The specimen contained matrix and solid lubricants, which were bonded. The density of AS matrix is 7,850 kg/m^3, elastic modulus is 209 GPa, strain rate parameter is 0.008, and Poisson's ratio is 0.30. The elastic modulus of solid lubricants is 39.5 GPa and Poisson's ratio is 0.28. The lower surface of specimen was fixedly supported. A uniform positive pressure of 1,057 MPa, which was consistent with the tribological test, was applied to the tribo-pair above. The meshes of specimen were divided by tetrahedron, and meshes qualities were mainly distributed in 0.7–1.0, which could ensure the high accuracy of simulated experiences. In addition, the design region and exclusion region were set in model, which could ensure the optimization of design in the unit cell structure.

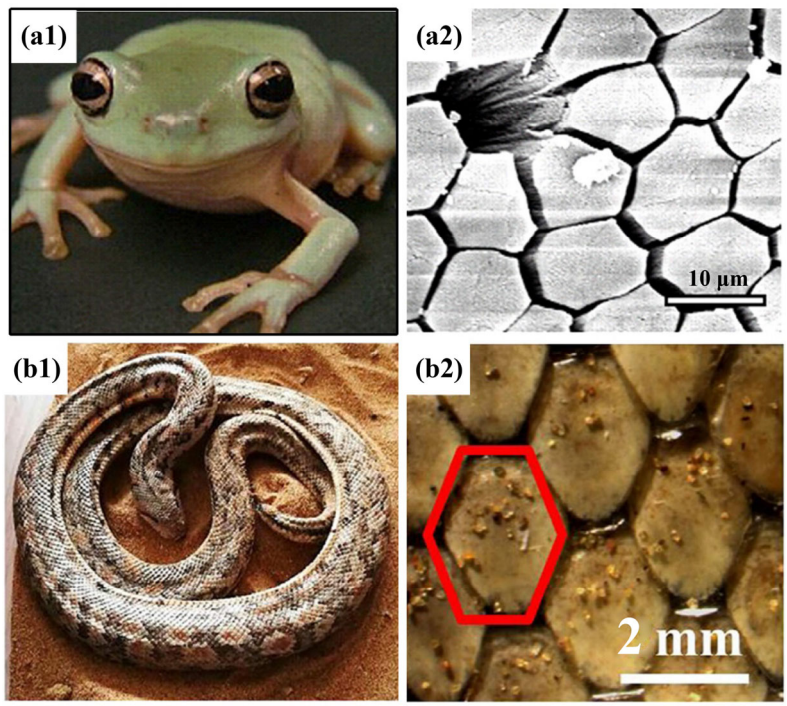

Fig. 1 (a1) Tree frog and (a2) surface texture of its toes; (b1) snake and (b2) its scale structure. For (a1) and (a2), reproduced with permission from Ref. [7] © Elsevier Ltd. 2023; for (b1) and (b2), reproduced with permission from Ref. [37] © Elsevier Ltd. 2018.

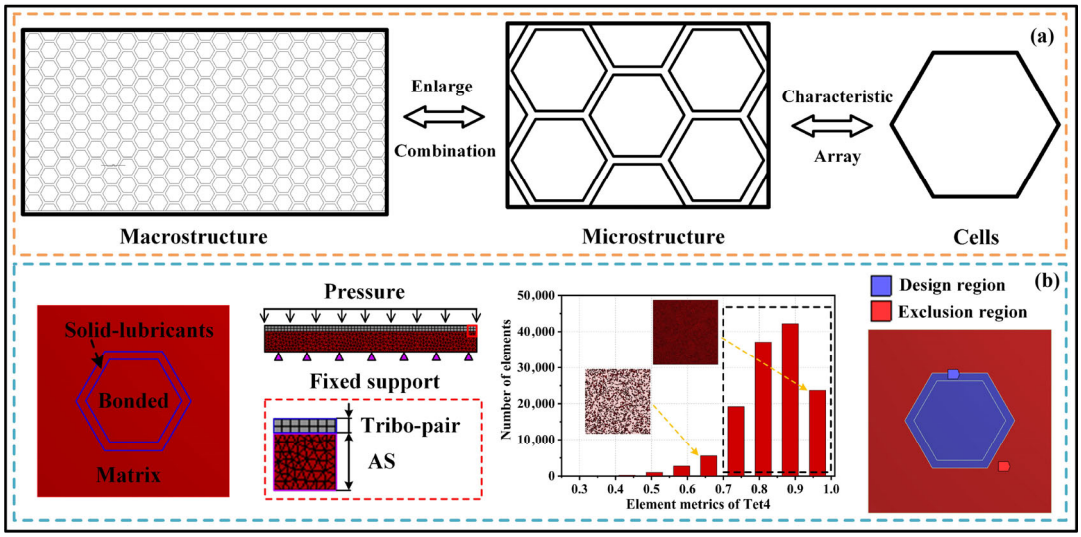

Fig. 2 (a) Extraction of cell structure and (b) parameter setting process of topology optimization.

According to the texture classification of self-lubricating materials by Huang et al. [7], the texture densities of steel surface are usually 5%–40%. In the equivalent stress results of the obtained cell structures, 5%, 10%, 20%, 25%, 30%, 35%, and 40% of the material were removed to obtain the optimized topologies, respectively (Fig. 3). In order to facilitate the processing and parameter design of the surface texture, the material removal areas were designed as regular geometry. When the material was removed by 5%–20%, cell region could be simplified to a circle. When the material removal was 25%–40%, cell region was a composite structure of circle and hexagon. The prototype of bionic texture was hexagon, which was set as the control group. Therefore, three types of texture were designed, including circle (C), hexagon (H), and circle/hexagon (CH)).

2.3 Parameter design of topological surface

Figure 4 showed the distributions of C, H, and topological surfaces of CH. Texture parameters included the radius (r) of circle, the circumcircle (R) of hexagon, the distance (a) between center and center of circles, and surface texture density (ε). Texture

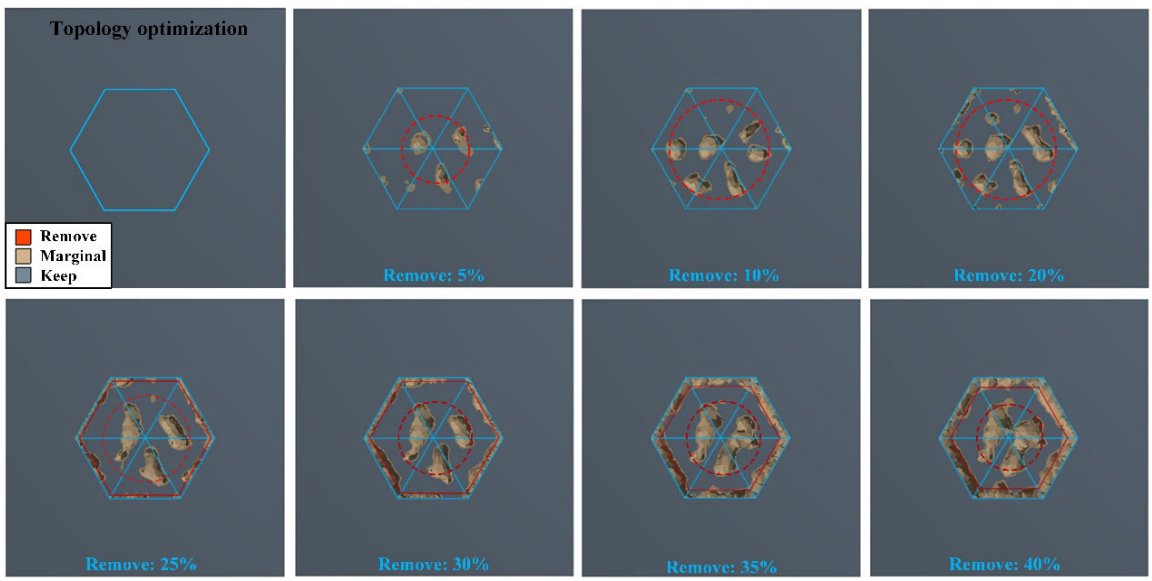

Fig. 3 Topological surfaces obtained by removing 0, 5%, 10%, 20%, 25%, 30%, 35%, and 40% of the material.

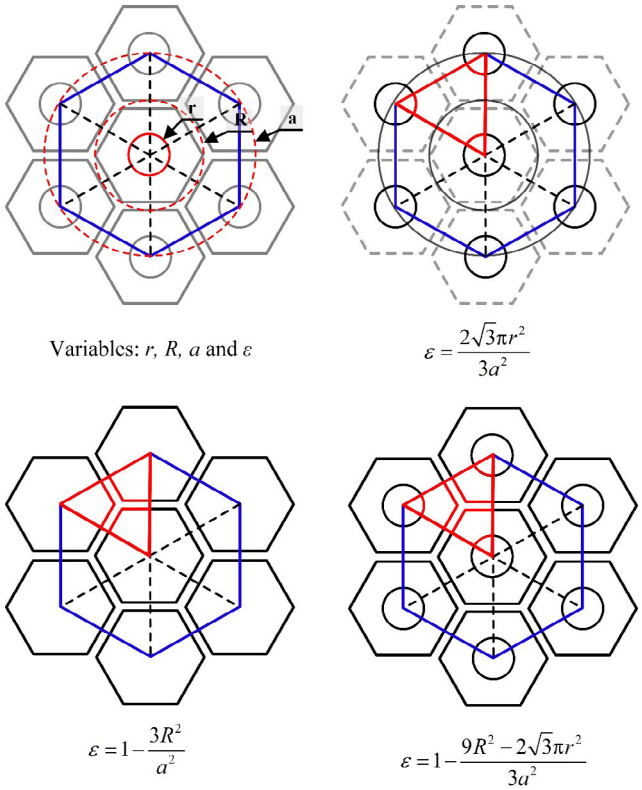

Fig. 4 Distributions and mathematical models of C, H, and CH.

density was the proportion of surface texture area to whole surface, which was one of important indexes affecting the tribological properties. In order to study the effect of different texture types on tribological properties of AS, mathematical models (Eqs. (1)–(3)) of texture parameters in three texture types were established, respectively.

Circular texture:

$$\varepsilon = \frac{2\sqrt{3}\pi r^2}{3a^2} \tag{1}$$

Hexagonal texture

$$\varepsilon = 1 - \frac{3R^2}{a^2} \tag{2}$$

Circular/hexagonal texture

$$\varepsilon = 1 - \frac{9R^2 - 2\sqrt{3}\pi r^2}{3a^2} \tag{3}$$

Based on the established mathematical model, the relational graphs between density and variable

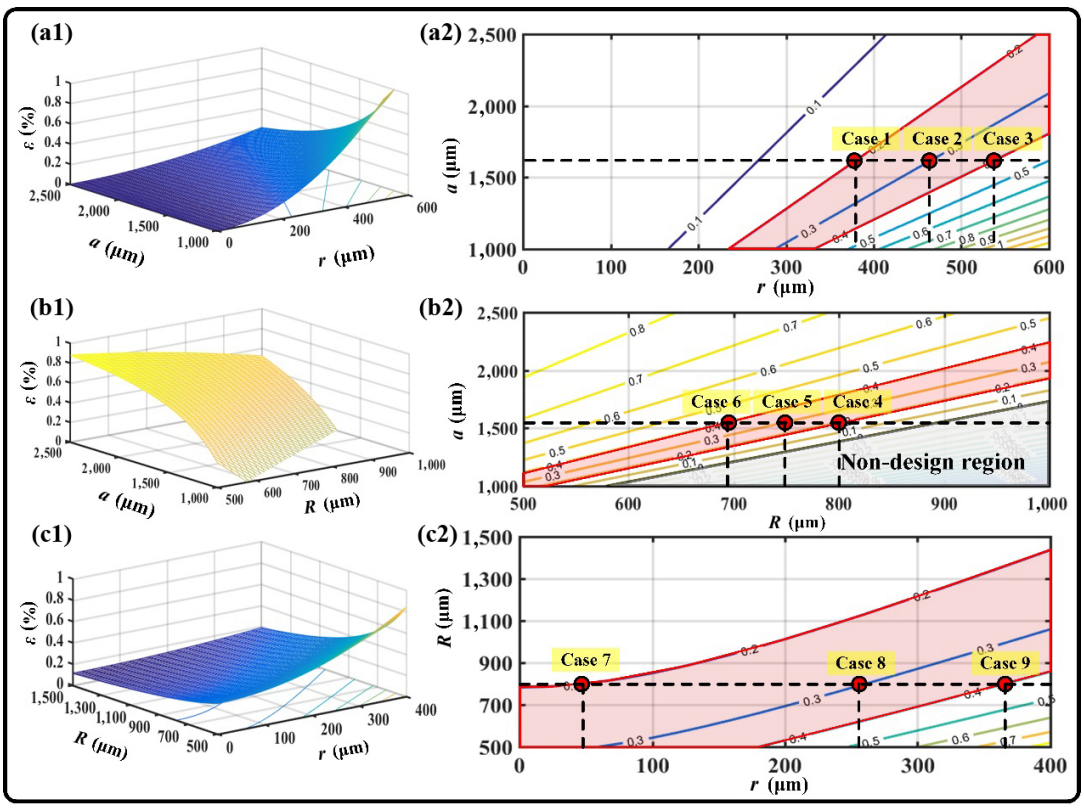

Fig. 5 Relational graphs between density and variable parameters, and their mappings at different texture densities (20%, 30%, and 40%) of (a1, a2) C, (b1, b2) H, and (c1, c2) CH.

parameters of circular texture (Fig. 5(a1)), hexagonal texture (Fig. 5(b1)) and circular/hexagonal texture (Fig. 5(c1)) were obtained using MATLAB, respectively. Previous studies [7, 41, 42] showed that low alloy steels with 20%–40% texture density could exert stable tribological properties. Therefore, three cases of of C (Fig. 5(a2)), H (Fig. 5(b2)) and CH (Fig. 5(c2)) with 20%, 30% and, 40% texture density were obtained in mappings, respectively. The detailed parameters of cases 1–9 were shown in Table 1. According to the mathematical parameters of Table 1, the macroscopic topological surface is obtained by the repeated iteration of microscopic cell structure. Figure 6 shows three- dimensional model of cases 1–9.

3 Experimental details

In order to confirm that the designed topological surface combined with multi-solid lubricants could regulate mechanical and tribological properties, nine types of self-lubricating materials were prepared and tested for tribological properties.

3.1 Preparation of materials

The preparation of self-lubricating materials included texture processing, fabrication of multi-solid lubricants and composite processing of self-lubricating materials. AS samples were provided by Xuzhou Wanda slewing bearing, and their specific size was 12 mm × 10 mm × 4 mm. The composition of AS mainly contains 0.42 wt% C, 0.95 wt% Cr, 0.17 wt% Mo, 0.74 wt% Mn, 0.20 wt% Mo, 0.22 wt% Si and Fe (balance). Commencing with the processing of topological surface (Fig. 7(a)), a 30 W fiber laser marking machine (LSF30D, HGTECH, China) with a wavelength of 1,064 nm and a fluence of 12.7 J/cm^2 was used to mark 12 mm × 10 mm surfaces to obtain samples with surface texture (Fig. 8). The specific processing parameters were 80% operating power, 500 mm/s scanning velocity, and 80 times repeated scanning. The repeated machining accuracy

Table 1 The detailed parameters of C, H, and CH with 20%, 30%, and 40% texture densities.

Density type	C (μm)	H (μm)	CH (μm)
20%	r=363, a=1545.6	R=798, a=1545.6	r=50, R=800, a=1545.6
30%	r=444, a=1545.6	R=747, a=1545.6	r=261, R=800, a=1545.6
40%	r=513, a=1545.6	R=691, a=1545.6	r=366, R=800, a=1545.6

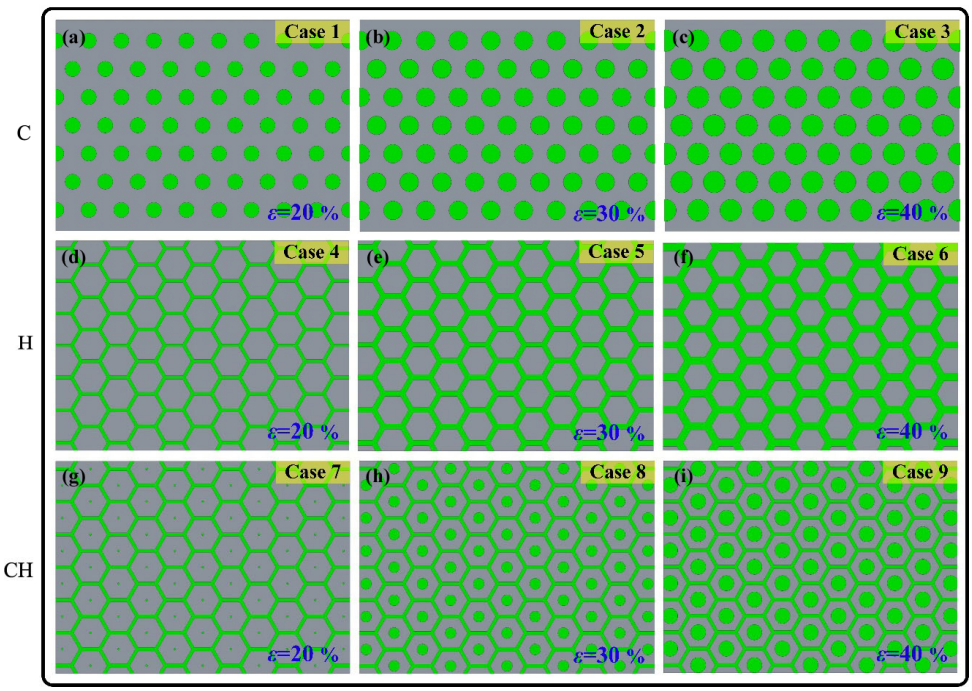

Fig. 6 Three-dimensional models of C, H, and CH with 20%, 30%, and 40% texture densities.

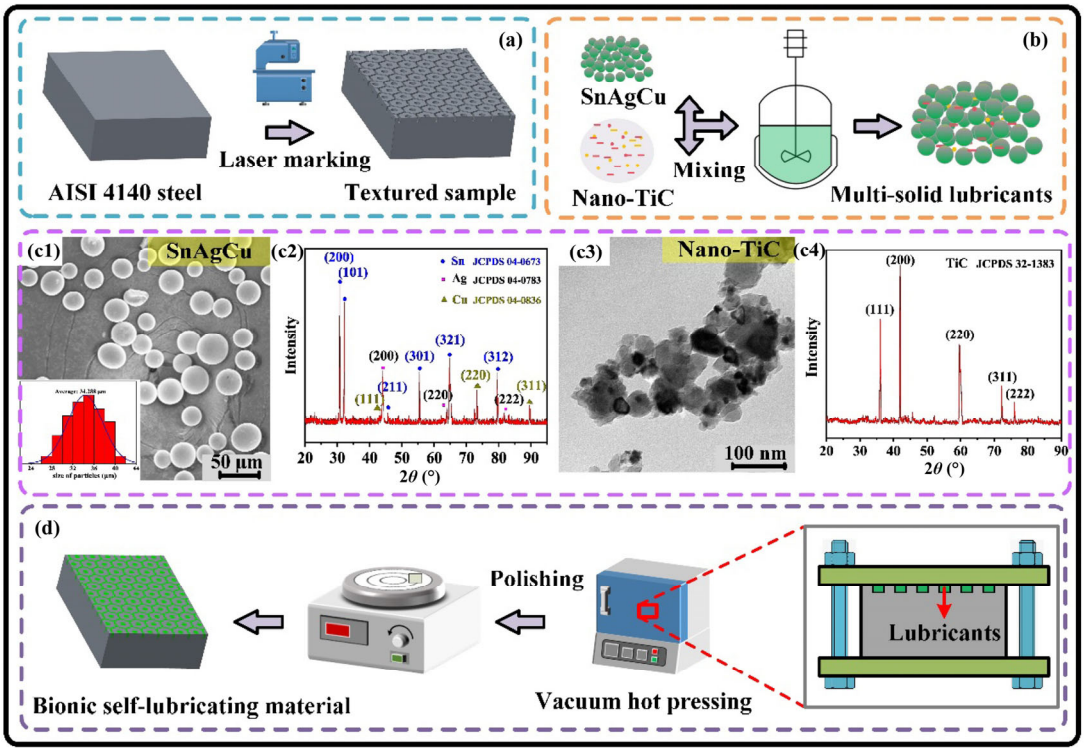

Fig. 7 (a) Processing of topological surface; (b) fabrication of multi-solid lubricants; morphology and XRD of (c1, c2) SnAgCu and (c3, c4) nano-TiC; (d) Preparation of self-lubricative materials.

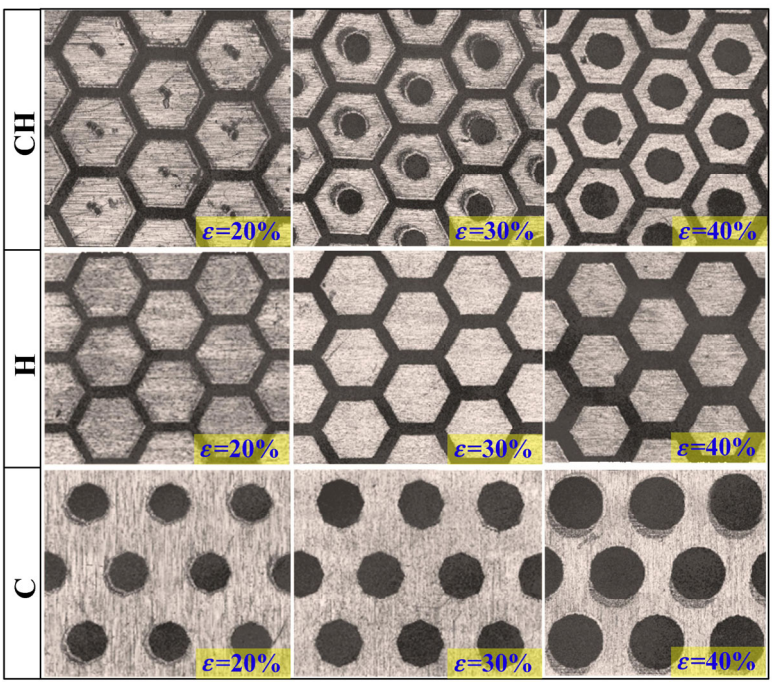

Fig. 8 The samples with C, H and CH textures at densities of 20%, 30%, and 40%

is 0.01 mm. After that, the surfaces of samples were polished to make the surface roughness less than 0.2 μm. Subsequently, the samples were cleaned in an ultrasonic cleaner with anhydrous ethanol for 10 min, and then they were dried with a hairdryer.

With regard to fabrication of multi-solid lubricants

(Fig. 7(b)), raw material powders of SnAgCu and nano-TiC were purchased commercially in China Shanghai Aladdin Biochemical Technology Co., Ltd. SnAgCu powders were composed of 96% Sn, 3.5% Ag and 0.5% Cu. The average diameter of SnAgCu was 34.288 μm (Fig. 7(c1)). XRD pattern of SnAgCu (Fig. 7(c2)) showed the diffraction peaks of Sn, Ag and Cu, and no other impurity peaks. The average diameter of nano-TiC was 50 nm (Fig. 7(c3)). XRD pattern of nano-TiC (Fig. 7(c4)) showed the diffraction peak of TiC without other impurity peaks. The next step was to mix raw material powders. The powders of 470 g SnAgCu and 30 g nano-TiC were put into ball mill for mechanical mixing. The parameters were set as 10,000 N vibration force, 10:1 ball material mass ratio and 120 min stirring time. After that, the mixed slurry was cleaned with deionized water and filtered using a stainless-steel mesh. Finally, the multi-solid lubricants of SnAgCu-TiC were obtained by vacuum drying oven.

AS self-lubricating materials (AS、AS-C20、AS-C20、AS-C20、AS-H20、AS-H30、AS-H40、AS-CH20、AS-CH30 and AS-CH40) were prepared by vacuum infiltration technology. The multi-solid lubricants were mixed with oleic acid to form a viscous substance and coated on the textured surfaces of samples. Next, they were tightened and placed in a vacuum pressure infiltration furnace for filling. The specific parameters were set as 0.1×10^{-2} Pa vacuum, 280 °C heating temperature, 40 min holding time, 0.8 MPa pressure and 90 min infiltration time. After being cooled to room temperature with the furnace, the samples were polished to make the roughness less than 0.2 μm, and the AS self-lubricating materials with different topological surfaces and multi-solid lubricants were obtained.

3.2 Tribological test

Tribological tests of all specimens were performed on a pin-on-disk reciprocating tribometer (MFT-5000, Rtec Instruments, USA) and instantaneous COFs were recorded in dry friction. The diameter of counterpart GCr15 ball against AS sample was 6.3 mm. The friction tests were carried out under the condition of 5 N normal load (contact pressure: 1,057 MPa), 2 Hz sliding speed, 8 mm reciprocating motion displacement and 20 min at room temperature. Each group of samples was tested three times. Wear track profiles were measured by a white light interferometer to obtain wear volume. In addition, the finite element method was used to simulate the equivalent stress of topological surface during the sliding process.

3.3 Material characterization

During the preparation of samples, the morphologies of SnAgCu spherical powders were observed by Electron probe microanalyzer (EPMA, JXA-8230, JEOL Corporation, Japan), and the diameters of spherical powders were measured by Image J software. The morphologies of nano-TiC were photographed using 120 KV transmission electron microscope (TEM, JEM-1400Plus, JEOL Corporation, Japan). SnAgCu and nano-TiC were identified by X-ray diffractometry (XRD, D/MAX-RB, RIGAKU Corporation, Japan). The morphologies of samples with different texture types were obtained using a metallographic microscope (RX50, Sunny Optical Technology Co., Ltd., China).

The mechanical properties were analyzed using Ansys Workbench 19.0. Electron probe microanalyzer with energy dispersive spectrometer (EPMA/EDS, JXA-8230, JEOL Corporation, Japan) was used to observe the microstructure, and analyze elemental contents and distributions of worn surfaces. The micromorphologies and roughnesses of samples and counterpart balls were photographed using white light interferometer (MFT-5000, Rtec Instruments, USA). The cross-sections, line elemental contents and wear debris of samples were analyzed by field emission scanning electron microscope with X-Max 50 X-ray spectrometer (FESEM, ULTRA-PLUS-43-13, Zeiss Corporation, Germany). The elemental compositions and chemical states of AS-CH30 were analyzed by X-ray photoelectron spectroscopy (XPS, ESCALAB 250 Xi, Thermo Fisher Scientific, USA).

4 Results and discussion

4.1 Tribological performance

In order to confirm that topological surface combined with multi-solid lubricants could improve tribological properties of AS, friction tests of AS self-lubricating

materials were carried out in dry friction. Figures 9(a)–9(d) showed the instantaneous COF curves of AS-C, AS-H, AS-CH and AS, respectively. As shown in Fig. 9, the friction process includes the running-in stage and stable wear stage. The running-in stages of AS, AS-C and AS-H were about 600 s, 300 s and 230 s, respectively, while the running-in stage of AS-CH was about 200 s. The COF of AS-C gradually increased after 600 s, while COFs of AS-H and AS-CH tended to be stable after 600 s. Compared with that of AS, the running-in stage of AS-CH was significantly shortened and reduced by 66.6%. It was worth mentioning that the COF of CH-30 was decreased to below 0.1 after 600 s, which was the lowest among all types of samples. Compared with AS, the COFs of topological surfaces were significantly reduced and the running-in stage was obviously shortened.

In addition to texture shape regulating tribological properties of AS self-lubricating materials, texture density also had a positive effect on the lubrication performance. Compared with those of AS self-lubricating materials with 20% and 40% texture densities, the COF of AS self-lubricating materials with 30% texture density was the lowest, indicating that surface texture density had a promoting effect on antifriction. Solid self-lubricating materials had an optimal texture density [6, 7]. When the texture density was higher than a specific value, the increasing boundary of friction surface would produce stress concentration and aggravate friction. On the contrary, the low-density textured samples increased the bite force of contact interface and can not be effectively lubricated. Figures 9(e) and 9(f) showed the average COFs and wear rates of AS self-lubricating materials, respectively. The average COF and wear rate of AS-CH30 were the smallest. Compared with the average COF of AS (0.438), the average COF of CH30 (0.089) was decreased by 79.68%. Compared with that of AS (146), the wear rate of CH30 (32) was decreased by 78.00%.

4.2 Mechanical performance

During the process of sliding friction, the stress distribution on the contact surface is an important index to evaluate the bearing capacities of specimens. The AS self-lubricating materials with a texture density of 30% had a low COF (Fig. 9). For revealing the effect of bionic topological surface on mechanical properties, the equivalent stresses of different textures with 30% density (AS, AS-C30, AS-H30 and AS-CH30) were analyzed by transient dynamic simulation of Ansys Workbench 19.0. The parameters of specific simulation samples are consistent with the sizes of test samples (Fig. 8). The transient dynamic parameters were set as follows: 1 s reciprocating time, 5 N load

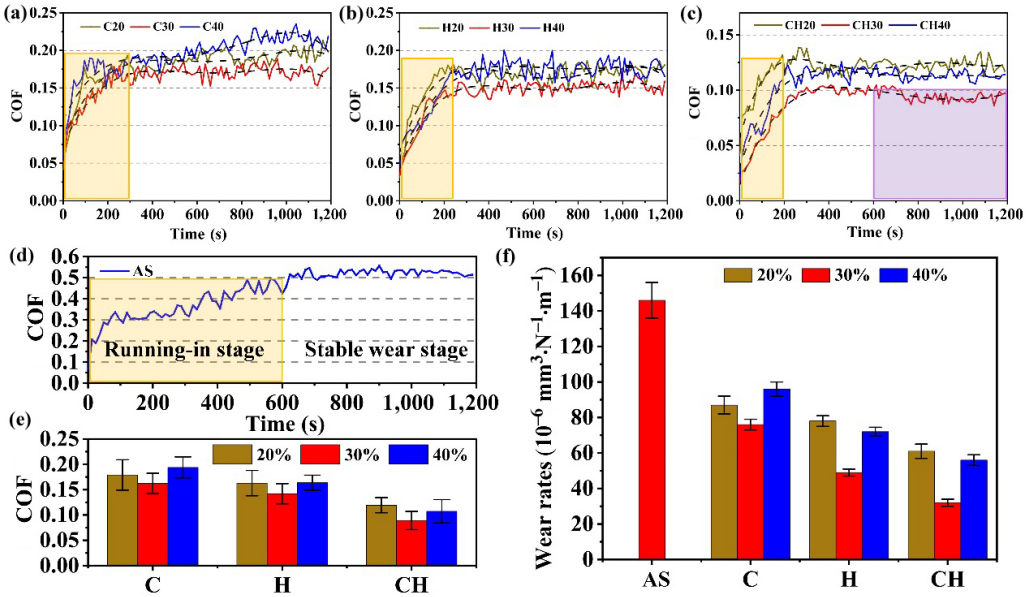

Fig. 9 The instantaneous COF curves of (a) AS-C, (b) AS-H, (c) AS-CH, and (d) AS; the (e) average COFs and (f) wear rates of AS self-lubricating materials

and 32 cm/s sliding speed. The material of sample was AS. Its density was 7,850 kg/m^3, elastic modulus was 209 GPa, strain rate parameter was 0.008, and Poisson's ratio was 0.30 (Fig. 10(a)). The mesh was divided by tetrahedron, and its mesh quality is mainly distributed in 0.7–1.0, which could ensure the high accuracy of simulated results (Fig. 10(b)). The input simulation COF is the average COF measured in Fig. 9.

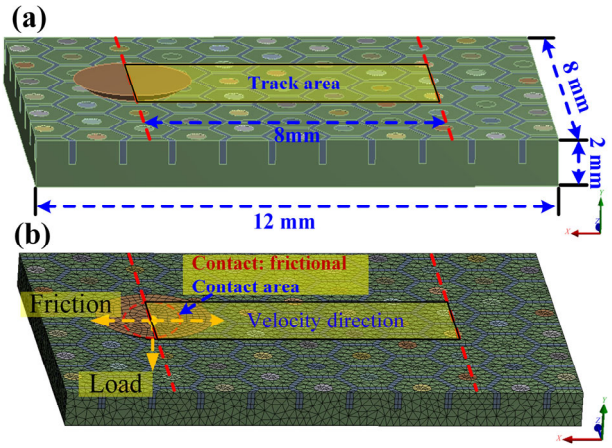

Fig. 10 Transient dynamics parameter (a) setting and (b) meshing.

The equivalent stress distributions of samples at the contact interface were periodic. Figure 11 showed four instantaneous stress states of a single period from *X*1 to (*X*1+1.345) m. During the sliding process, the maximum equivalent stress area was obtained when running to (*X*1+0.445) m. The maximum equivalent stresses of AS, AS-C30, AS-H30, and AS-CH30 were 5.85 GPa, 14.82 GPa, 13.95 GPa, and 13.21 GPa, respectively. Compared with the maximum equivalent stresses of AS-C and AS-H, the equivalent stress of AS-CH was decreased by 10.86% and 5.37%, respectively. In addition, stress cloud diagram (Figs. 11(b2)–11(d2)) showed that stress concentration area appeared at the edge of texture. The stress of AS-CH30 was mainly distributed near circular texture in the initial position (*X*1), then gradually extended to the edge of the hexagon (*X*1+0.445) m, and finally the stress was relatively dispersed on the contact surface from (*X*1+ 0.89) m to (*X*1+1.345) m. There was no doubt that the surface texture of substrate would increase the surface stress, but the topology surface could reduce the stress concentration to a certain extent.

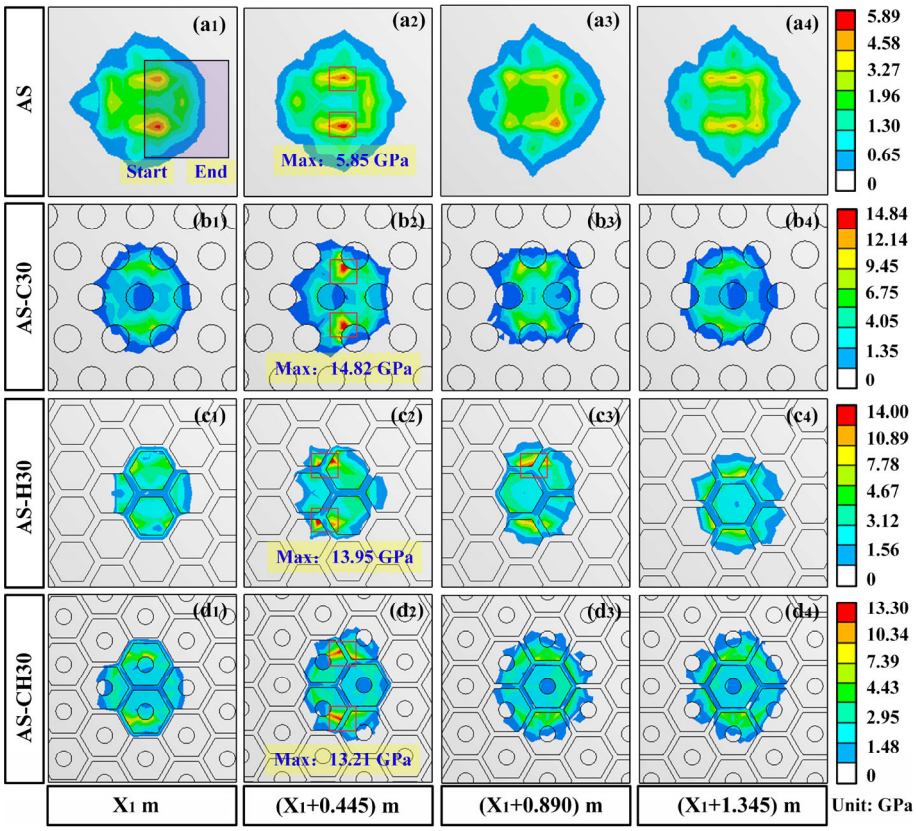

Fig. 11 Equivalent stress contours of (a) AS, (b) AS-C30, (c) AS-H30, and (d) AS-CH30 from *X*1 to (*X*1+1.345) m.

In order to explore the effects of topological texture on counterpart balls, the equivalent stress contours of counterpart balls against AS, AS-C30, AS-H30 and AS-CH30 at ($X1$ + 0.445) m were shown in Fig. 12. The maximum stress values of AS, AS-C30, AS-H30, and AS-CH30 were 38.75 GPa, 42.24 GPa, 32.05 GPa, and 29.16 GPa, respectively. Compared with those of AS-C30 and AS-H30, the maximum equivalent stress of AS-CH30 were reduced by 30.96% and 9.01%, respectively. It can be seen that the low-stress regions (blue) of AS-H30 and AS-CH30 were increased significantly from the cloud maps. Therefore, the bionic topological texture reduced the maximum stresses of counterpart balls and increased the low-stress distribution area.

In order to further investigate the effect of topological surface on the stresses of samples, the maximum equivalent stress curves of AS, AS-C30, AS-H30 and AS-CH30 and their counterpart balls were given in Fig. 13. Among these data, the stress of AS was the smallest, while that of counterpart ball against AS was higher, leading to more severe friction and wear phenomenon of counterpart ball against AS. Stress distribution refers to the force on the surface and inside of the object under loading, which is not only related to the properties and geometries of materials, but also related to the load. In the case of similar force field, the non-smooth transition (texture) of contact surface was main reason for stress concentration. Therefore, AS with smooth surface had low surface stress. For counterpart balls against AS, AS-C30, AS-H30, and AS-CH30, the equivalent stress of counterpart ball against AS was higher. The equivalent stress fluctuations and values of AS-C30 and its counterpart ball were the largest among all samples. Compared with that of AS-C30, the equivalent

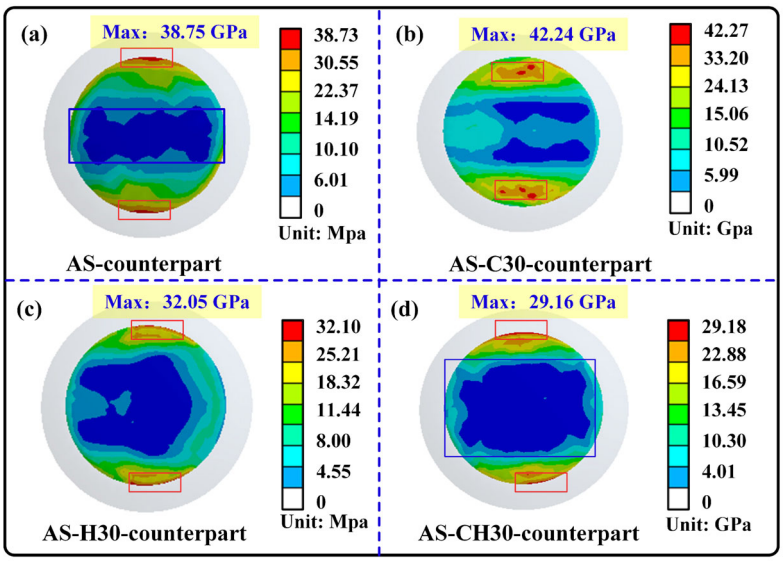

Fig. 12 Equivalent stress contours of counterpart balls against (a) AS, (b) AS-C30, (c) AS-H30, and (d) AS-CH30 at ($X1$ + 0.445) m.

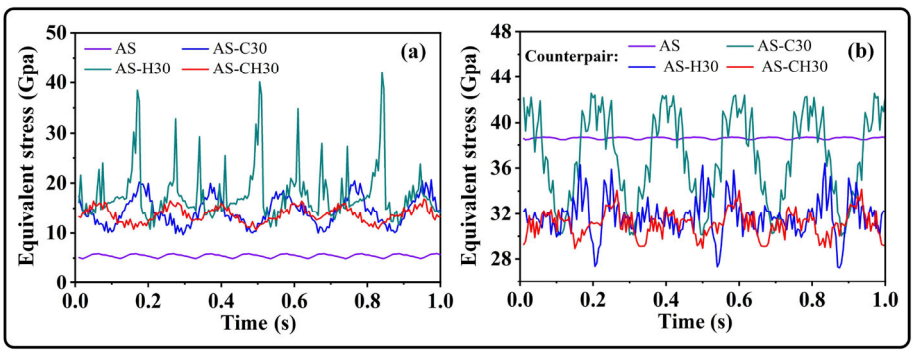

Fig. 13 The maximum equivalent stress curves of (a) AS, AS-C30, AS-H30, and AS-CH30, and (b) their counterpart balls.

stresses of AS-H30 were declined. It was worth noting that equivalent stress change trends of AS-C30 and AS-H30 were opposite in the same time, which made the equivalent stresses and fluctuation range of AS-CH30 with circular/hexagonal texture and its counterpart ball be significantly plunged during the friction process. Compared with those of AS-C30 and AS-H30, the equivalent stresses of AS-CH30 with bionic topological surface were the lowest. AS-H30 with topologically optimized surfaces have excellent anti-friction and wear resistance, which was attributed to the fact that topological surface not only adjusted the stress distribution at contact interface, but also inhibited the occurrence of dislocations to a certain extent, thereby alleviating the deformation and removal of nanoscale materials to reduce surface wear and subsurface damage [11, 42].

4.3 Worn surface and transfer film analyses

AS-CH30 with topological surface and multi-solid lubricants had low COF, low wear rate, and excellent mechanical properties. In order to clarify the anti-friction mechanism of AS-CH30, worn surfaces were researched and analyzed. Before wear, solid lubricant area and matrix area on the surface of AS-CH30 have a clear boundary (Fig. 14(a)). After wear, some small pits appeared in the hexagonal texture region (Fig. 14(b)). Surface element scanning mappings (Fe, Sn, Ag, and Cu) confirmed that some solid lubricants existed obviously on the surface of hexagonal matrix, indicated that there was material transfer process between matrix material and multi-solid lubricants during the friction process.

Atomic diffusion is the transposition and movement of atoms caused by the movement of atoms breaking the position constraint of crystals, which is driven by chemical potential gradient of components. Iron atom in the carbon steel is inactive element which is difficult to diffuse, and Sn atom in solid lubricants is active element which is easy to diffuse. Under the action of chemical potential energy, solid lubricants dominated by tin atoms diffuse to the worn surface of AS during the friction process [32]. In order to clarify the material transfer process of matrix and solid lubricants, worn surfaces of AS-CH30 were studied. The transfer phenomenon of multi-solid lubricants on the worn surface was observed (see Fig. 15(a)). Near the solid lubricants in texture, some solid lubricants adhered to matrix surface, which was confirmed by the back-scattering mappings and surface element distributions of Fe and Sn. Matrix elements (Fe, Cr, etc.) and a large number of solid lubricant elements (such as Sn, Ag, and Ti) were found by point element scanning of matrix region, which was caused by atomic diffusion. Driven by friction/heat, multi-solid lubricants in the texture were transferred to the worn surface.

Solid lubricant atoms gathered in a region to a certain concentration would form a lubricating film at the contact interface. Figures 15(b1) and 15(b2) showed a lubricating layer was observed. Line element scanning (Fe, Sn, and O) was performed by amplifying the local

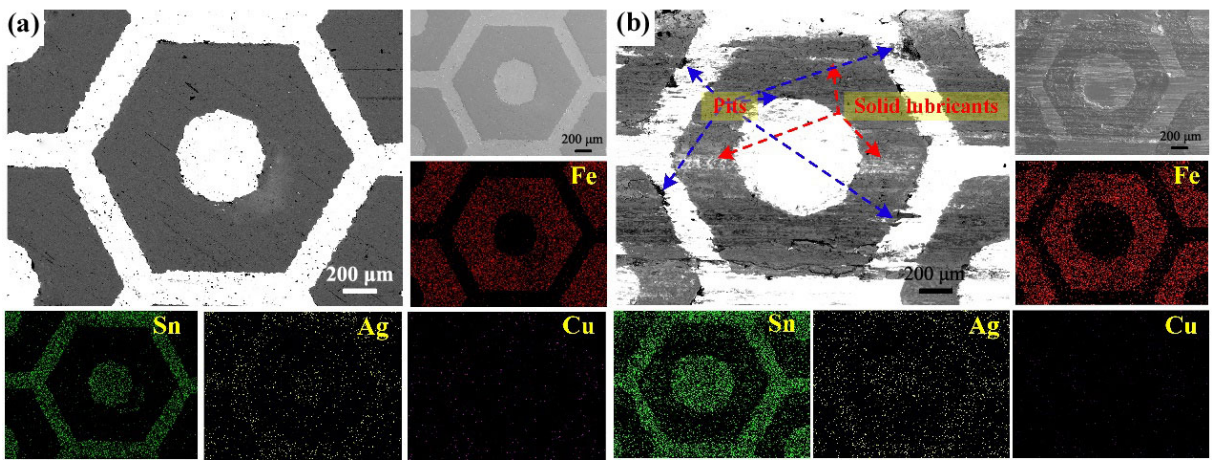

Fig. 14 Back scattering images, surface morphologies and elemental distributions (Fe, Sn, Ag, and Cu) of AS-CH30: (a) before wear and (b) after wear.

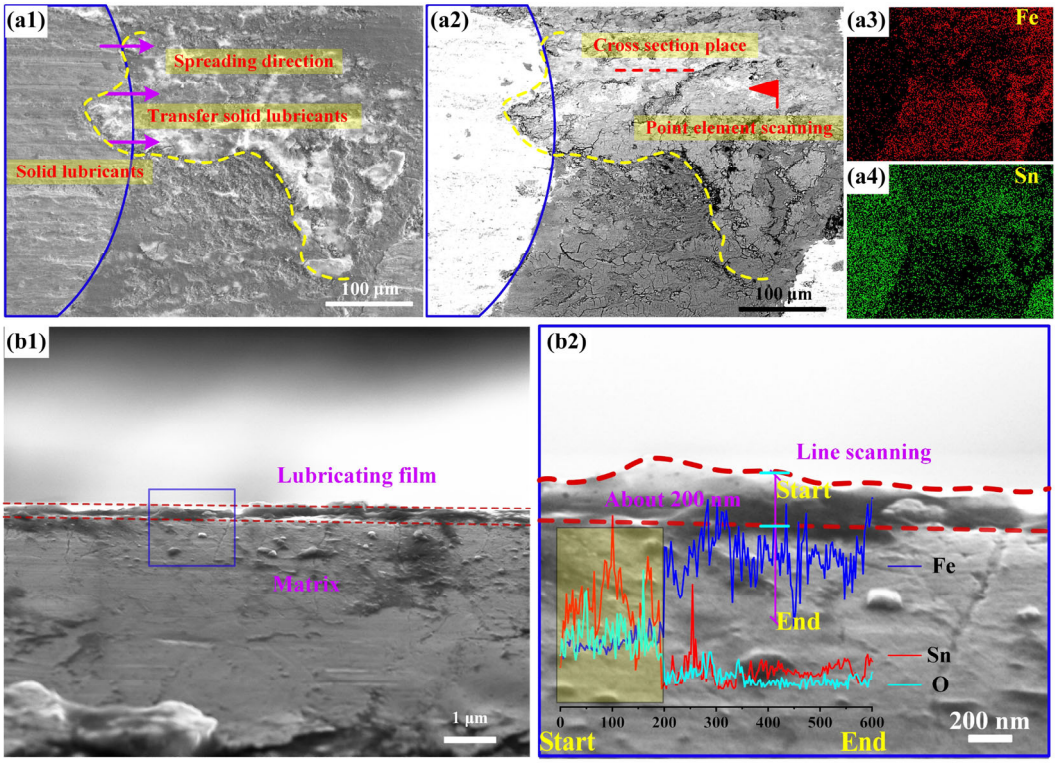

Fig. 15 (a1) Typical wear track, (a2) backscattered map, and (a3, a4) element surface scanning mappings (Fe and Sn) of AS-CH30; (b1) the cross-section and (b2) local magnification map of AS-CH30.

area of the lubricating film. Sn (lubricant element) and O remained stable from 0 to 200 nm and then decreased sharply. Fe element (matrix element) rose quickly after 200 nm. During the friction process, the solid lubricants stored in texture were driven by shear force and/or friction heat to spread to worn surface.

XPS results in the lubricating film area confirmed the presence of TiC, TiO_2, FeO, Fe_2O_3, SnO_2, and AgO. The peak position of C 1s combined with the Ti 2p spectrum can be judged that Fig. 16(a) corresponds to the Ti–C bond. The chemical binding energies of the O 1s peak are 531.88 eV and 529.28 eV, indicating that there are two different valence states of oxides (Fig. 16(b)). The presence of FeO and Fe_2O_3 may be attributed to the material transfer of AS matrix, indicating that the lubricating film in the wear track was composed of wear debris, solid lubricants and oxides produced by tribochemical reaction (Fig. 16(c)). In Fig. 16(d), Sn $3d_{5/2}$ and $3d_{3/2}$ were located at 486.28 eV and 494.68 eV, respectively, confirming the existence of SnO_2 [43]. In the Ag 3d spectra (Fig. 16(e)), Ag $3d_{5/2}$ and $3d_{3/2}$ peaks appear at 368.6 eV and 374.6 eV, respectively. Compared with the characteristic peaks of silver (368.2 eV and 374.2 eV), they move to higher binding energy. Ag $3d_{5/2}$ binding energies of Ag, Ag_2O, and AgO are 368.2, 367.4, and 367.8 eV, respectively [44]. Therefore, the increase of binding energy of Ag $3d_{3/2}$ and Ag $3d_{5/2}$ may be due to the slight oxidation of Ag. The oxides of Ag have been proved to have excellent antifriction effect. In the spectrum of Ti 2p, TiC and TiO_2 were obtained, indicating that nano-TiC was oxided by the tribochemical reaction during the friction process (Fig. 16(f)). Therefore, the multi-solid lubricants were transferred from topological texture to the friction interface to form a lubricating film containing solid lubricants (mainly), oxides and wear debris.

After friction test, the pits on worn surface of AS-CH30 mainly existed three locations (see Fig. 17(a)). The pits with different sizes existed in the boundary positions of textures, and there were some peeling layers near the pits on worn surfaces. Some residual wear debris can be clearly observed in pits (see Fig. 17(e)). During the friction process of 0–1,200 s, the wear mechanism of AS self-lubricating material changed from abrasive wear to adhesive wear. It was found that wear debris

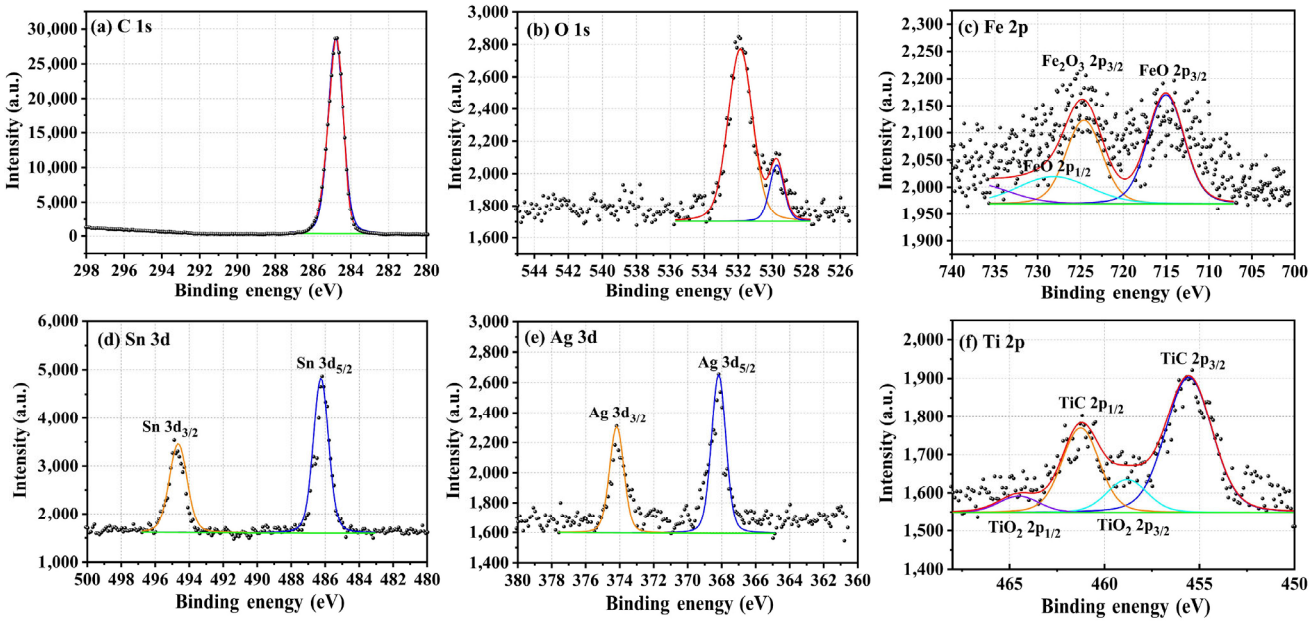

Fig. 16 XPS spectra: (a) C 1s spectrum, (b) O 1s spectrum, (c) Fe 2p spectrum, (d) Sn 3d spectrum, (e) Ag 3d spectrum and (f) Ti 2p spectrum.

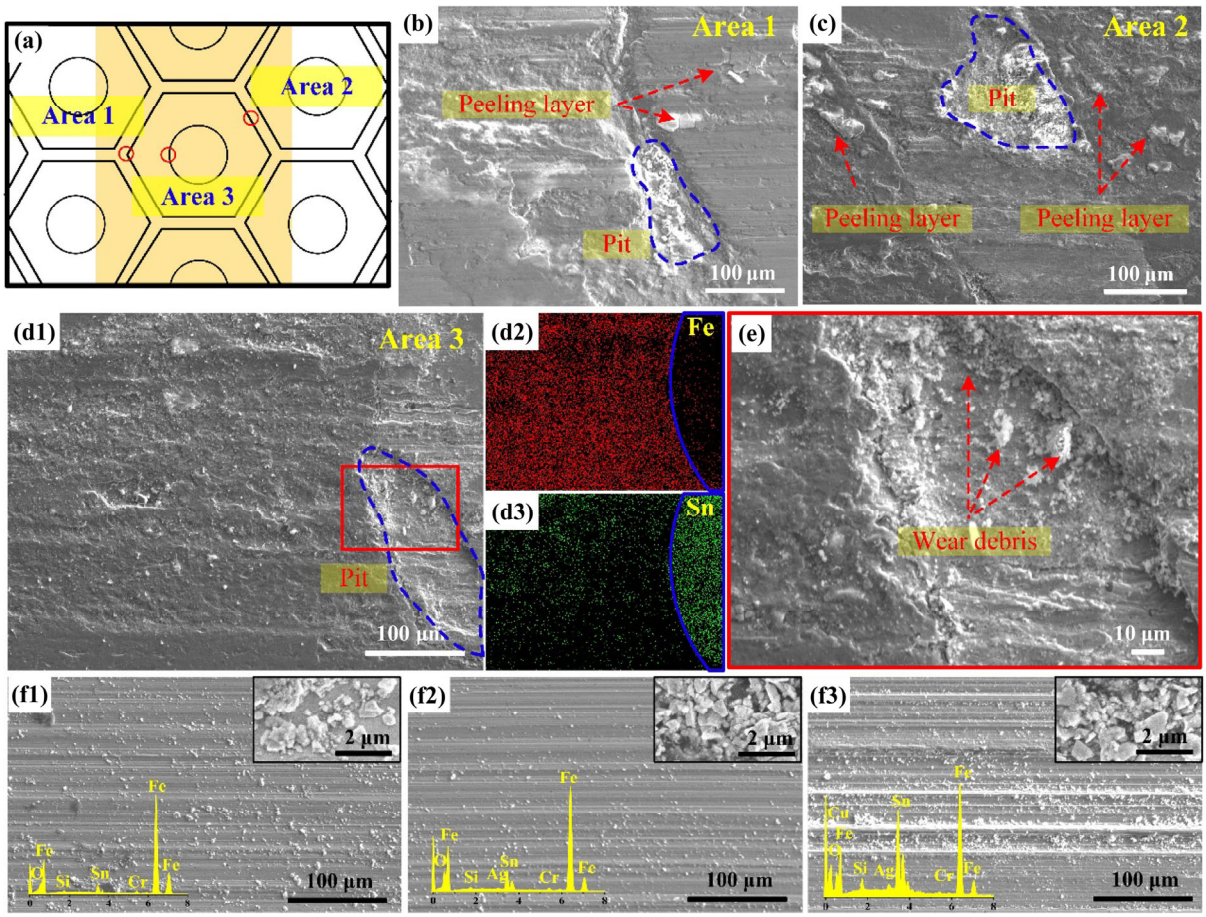

Fig. 17 (a) Diagram of wear track; wear track characteristics of (b) area 1, (c) area 2 and (d1) area 3; distribution diagram of (d2) Fe and (d3) Sn in area 3; (e) local amplification map of the area marked with the red rectangle in (d1) area 3; wear tracks and stored wear debris of (f1) AS-CH20, (f2) AS-CH30 and (f3) AS-CH40 at 600 s.

of AS-CH20, AS-CH30 and AS-CH40 were clearly distinguished at 600 s (Figs. 17(f1)–17(f3)). Compared with those of AS-CH20 and AS-CH40, the number and volume of wear debris on the worn surface of AS-CH30 were the smallest. Based on the element scanning results of wear debris, it was found that the solid lubricant elements (Sn and Ag, etc.) on the worn surface of AS-CH20 were few, while wear debris on the worn surface of AS-CH40 consisted of a large number of matrix elements (Fe, Cr, Si, etc.) and solid lubricant elements (Sn, Ag, etc.). In addition, massive O element was detected in the wear debris of AS-CH40. The excellent antifriction and wear resistance of AS-CH30 is attributed to the formation of a variety of hexagonal intermetallic compounds in the oxidation reaction, such as Ag_2Sn, Fe_3Sn_2, AgO and SnO_2, etc. [10].

The topological texture combined with multi-solid lubricants played a good role in antifriction and wear resistance for not only AS self-lubricative materials, but also their counterpart balls. Figure 18(a) showed the wear profiles of AS, AS-C30, AS-H30 and AS-CH30. The worn surface of counterpart ball against AS had obvious furrows, indicating that serious abrasive wear occurred on the worn surface. The contact surface of counterpart ball against AS-CH30 was only slightly worn. Figure 18(b) was the contour curves extracted from the worn surfaces of counterpart balls. The maximum height differences of AS, AS-C30, AS-H30 and AS-CH30 were 11.70 μm, 9.38 μm, 7.30 μm, and 5.57 μm, respectively, and the standard deviations were 2.07 μm, 1.61 μm, 1.28 μm, and 1.23 μm, respectively. Compared with those of AS, the maximum height difference and standard deviation of AS-CH30 were reduced by 52.39% and 40.58%, respectively. During the friction process, solid lubricants in the bionic topological texture could be transferred to the worn surfaces of AS-CH30 and its counterpart ball to form a lubricating film (Fig. 18(c)). These solid lubricating film with small shear force can reduce the contact points of the tribo-pairs, so that AS-CH30 and its counterpart ball have excellent wear resistance. Therefore, the surface texture combined with solid lubricants could have the excellent antifriction and wear resistance performance.

4.4 Discussion of the mechanisms

In view of the low COF and wear rate of AS-CH30, it could be concluded that the topological surface combined with multi-solid lubricants (SnAgCu-TiC) had the excellent effect of antifriction and wear resistance. Based on the above research results, the lubrication mechanisms of AS-CH30 could be obtained, as illustrated in Fig. 19. The friction diagram of AS-CH30 was shown in Fig. 19(a). In terms of improving mechanical properties, the macroscopic contact surface was divided into regions of closed circular texture and continuous hexagonal texture through cell topology optimization. The equivalent stress trends of AS-C with circular texture and AS-H with hexagonal texture were opposite, and the circular/

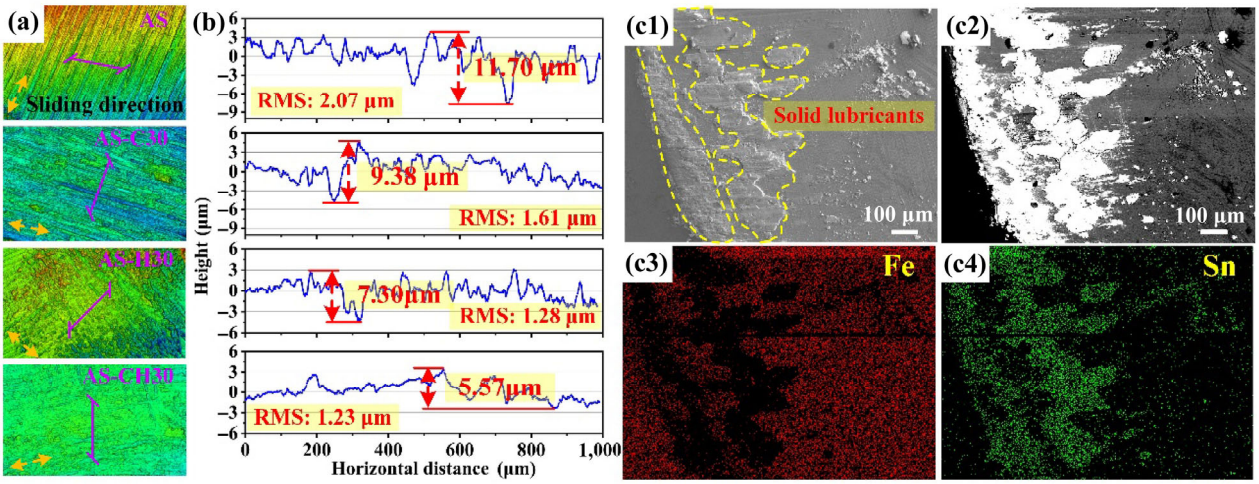

Fig. 18 (a) Wear profiles and (b) profile curves of AS, AS-C30, AS-H30 and AS-CH30; (c1) wear track characteristics, (c2) backscattered map, and (c3, c4) surface element scanning maps (Fe, Sn) of AS-CH30.

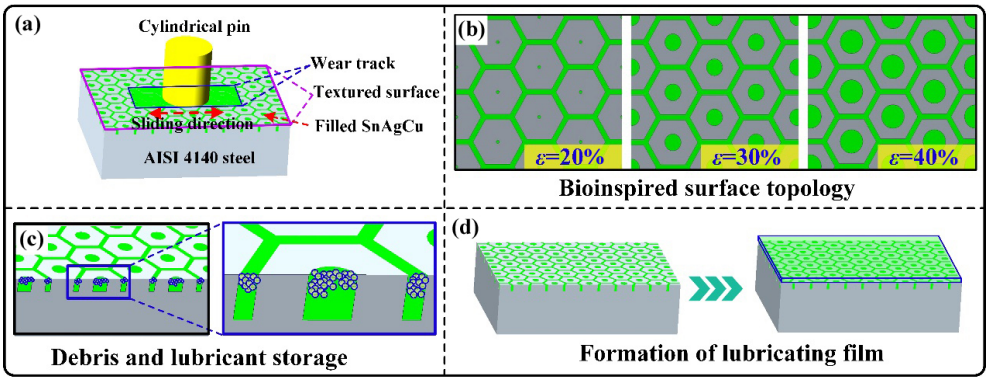

Fig. 19 (a) The friction diagram; (b) Bioinspired surface topology; (c) Wear debris and lubricant storage; (d) Formation of lubricating film.

hexagonal texture could weaken the equivalent stress and fluctuation. Therefore, the mechanical performance of AS-CH 30 was enhanced by reducing the stress at the contact interface (Fig. 19(b)). Topological textures not only adjust the stress distribution at the contact interface, but also inhibit the occurrence of dislocations to a certain extent, thereby alleviating the deformation and removal of nanoscale materials to reduce surface wear and subsurface damage [45]. 30% topological texture can provide sufficient coverage for multi-solid lubricants to effectively decline friction and wear.

Topological texture combined with the multi-solid lubricants (SnAgCu-TiC) with low interlaminar shear strength can play a synergistic effect to improve tribological properties. On the one hand, the precipitation rate of solid lubricants near the edge of texture was higher than that of middle region, resulting in a large number of small pits at the edge of texture. During the sliding process, the micro-pits can easily capture wear debris from worn surface, thereby reducing three-body wear (Fig. 19(c)). On the other hand, the multi-solid lubricants were transferred from topological texture to the friction interface to form a nano-scale lubricating film (about 200 nm) containing TiC, TiO_2, FeO, Fe_2O_3, SnO_2, AgO, etc. (Fig. 19(d)). Therefore, AS-CH30 obtains the excellent mechanical and tribological properties for the synergistic effect of topological surface and multi-solid lubricants.

5 Conclusions

Herein, nine types of AS self-lubricating materials were designed and prepared. Through the analysis of mechanical and tribological properties of samples, the following conclusions were obtained:

(1) Compared with those of AS-C and AS-H, the equivalent stress of AS-CH was decreased by 10.86% and 5.37%, respectively. Compared with that of counterpart ball against AS-C, the maximum equivalent stress of counterpart ball against AS-CH was reduced by 30.96%.

(2) Compared with these of AS, the average COF and wear rate of AS-CH30 were reduced by 79.68% and 78%, respectively. AS-CH30 showed the excellent anti-friction and wear resistance performances.

(3) The excellent tribological performances of AS-CH30 can be attributed to the synergistic effect of topological surface and multi-solid lubricants. Topological surface can not only reduce value and fluctuation of equivalent stress, but also promote the stored lubricants to be easily transferred at the contact interface to form a 200 nm solid lubricating film.

Acknowledgments

This work is supported by the National Natural Science Foundation of China (52375201) and Project for Science and Technology Plan of Henan Province (242102221026, 242102220054). Authors are also grateful to Xiaolei NIE, Yumei LI, Meijun YANG, Wanting ZHU, Suling ZHAO, and Linqin QIN in Material Research and Test Center of WUT for their kind help with SEM, EPMA, FESEM.

Declaration of competing interest

The authors have no competing interests to declare that are relevant to the content of this article.

References

[1] Jin X, Chen Y M, Wang L, Han H L, Chen P. Failure prediction, monitoring and diagnosis methods for slewing bearings of large-scale wind turbine: A review. *Measurement* **172**: 108855 (2021)

[2] Kandukuri S T, Klausen A, Karimi H R, Robbersmyr K G. A review of diagnostics and prognostics of low-speed machinery towards wind turbine farm-level health management. *Renew Sustain Energy Rev* **53**: 697–708 (2016)

[3] Zhai W Z, Bai L C, Zhou R H, Fan X L, Kang G Z, Liu Y, Zhou K. Recent progress on wear-resistant materials: Designs, properties, and applications. *Adv Sci* **8**(11): e2003739 (2021)

[4] Chen X, Han Z, Li X Y, Lu K. Lowering coefficient of friction in Cu alloys with stable gradient nanostructures. *Sci Adv* **2**(12): e1601942 (2016)

[5] Yan X C, Yang X, Qi X W, Lu G F, Dong Y, Liu C X, Fan B L. Tribological properties of PAO40@SiO_2/PTFE/aramid fabric composites subjected to heavy-loading conditions. *Tribol Int* **166**: 107336 (2022)

[6] Rosenkranz A, Costa H L, Baykara M Z, Martini A. Synergetic effects of surface texturing and solid lubricants to tailor friction and wear–A review. *Tribol Int* **155**: 106792 (2021)

[7] Huang Q P, Shi X L, Xue Y W, Zhang K P, Wu C H. Recent progress on surface texturing and solid lubricants in tribology: Designs, properties, and mechanisms. *Mater Today Commun* **35**: 105854 (2023)

[8] Rosenkranz A, Marian M. Combining surface textures and MXene coatings—Towards enhanced wear-resistance and durability. *Surf Topogr*: *Metrol Prop* **10**(3): 033001 (2022)

[9] Zhang K P, Shi X L, Xue Y W, Huang Q P, Wu C H. Effects of composite textured surface on friction characteristics of 42CrMo steel under grease lubrication. *Wear* **504–505**: 204419 (2022)

[10] Xue Y W, Wu C H, Shi X L, Huang Q P, Ibrahim A M M. Effects of groove-textured surfaces filled with Sn-Ag-Cu and MXene-Ti_3C_2 composite lubricants on tribological properties of CSS-42L bearing steel. *Friction* **10**(7): 1091–1113 (2022)

[11] Marian M, Almqvist A, Rosenkranz A, Fillon M. Numerical micro-texture optimization for lubricated contacts—A critical discussion. *Friction* **10**(11): 1772–1809 (2022)

[12] Rosenkranz A, Grützmacher P G, Gachot C, Costa H L. Surface texturing in machine elements—A critical discussion for rolling and sliding contacts. *Adv Eng Mater* **21**(8): 1900194 (2019)

[13] Zhang B J, Han Q G, Zhang J Q, Han Z W, Niu S C, Ren L Q. Advanced bio-inspired structural materials: Local properties determine overall performance. *Mater Today* **41**: 177–199 (2020)

[14] Chen P Y, McKittrick J, Meyers M A. Biological materials: Functional adaptations and bioinspired designs. *Prog Mater Sci* **57**(8): 1492–1704 (2012)

[15] Huang Q P, Shi X L, Xue Y W, Zhang K P, Wu C H. Wear-triggered self-repairing behavior of bionic textured AISI 4140 steel filled with multi-solid lubricants. *Wear* **504–505**: 204416 (2022)

[16] Zhang Y L, Zhao W Y, Ma S H, Liu H, Wang X W, Zhao X D, Yu B, Cai M R, Zhou F. Modulus adaptive lubricating prototype inspired by instant muscle hardening mechanism of catfish skin. *Nat Commun* **13**(1): 377 (2022)

[17] Huang Q P, Wu C H, Shi X L, Gao Y Y, Xue Y W, Zhang K P, Tang H T. Tribological properties of AISI 4140 steel reinforced by bioinspired topological texture and multi-solid lubricants under starved lubrication. *Tribol Int* **187**: 108692 (2023)

[18] Mao Y W, He Q, Zhao X H. Designing complex architectured materials with generative adversarial networks. *Sci Adv* **6**(17): eaaz4169 (2020)

[19] Meng X K, Tu Z R, Ma Y, Jiang J B, Peng X D. Topology optimization of liquid lubricating zero-leakage mechanical face seals. *Tribol Int* **169**: 107490 (2022)

[20] Grejtak T, Jia X, Feppon F, Joynson S G, Cunniffe A R, Shi Y P, Kauffman D P, Vermaak N, Krick B A. Topology optimization of composite materials for wear: A route to multifunctional materials for sliding interfaces. *Adv Eng Mater* **21**(8): 1900366 (2019)

[21] Jia X, Grejtak T, Krick B, Vermaak N. Topology optimization of tribological composites for multifunctional

performance at sliding interfaces. *Compos Part B Eng* **199**: 108209 (2020)

[22] Meng R, Deng J X, Liu Y Y, Duan R, Zhang G L. Improving tribological performance of cemented carbides by combining laser surface texturing and W-S-C solid lubricant coating. *Int J Refract Met Hard Mater* **72**: 163–171 (2018)

[23] Zhai W Z, Zhao Y J, Zhou R H, Lu W L, Zhai W C, Liu X J, Zhou L P, Chang S P. Additively manufactured (Fe, Ni)Al-reinforced nickel aluminum bronze with nearly-isotropic mechanical properties in build and transverse directions. *Mater Charact* **184**: 111706 (2022)

[24] Xing Y Q, Deng J X, Wang X S, Meng R. Effect of laser surface textures combined with multi-solid lubricant coatings on the tribological properties of Al_2O_3/TiC ceramic. *Wear* **342–343**: 1–12 (2015)

[25] Zhu S Y, Cheng J, Qiao Z H, Yang J. High temperature solid-lubricating materials: A review. *Tribol Int* **133**: 206–223 (2019)

[26] Kumar R, Hussainova I, Rahmani R, Antonov M. Solid lubrication at high-temperatures-a review. *Materials* (*Basel*) **15**(5): 1695 (2022)

[27] Chen Y, Yang K, Lin H B, Zhang F Z, Xiong B Y, Zhang H L, Zhang C H. Important contributions of multidimensional nanoadditives on the tribofilms: From formation mechanism to tribological behaviors. *Compos Part B Eng* **234**: 109732 (2022)

[28] Rosenkranz A, Righi M C, Sumant A V, Anasori B, Mochalin V N. Perspectives of 2D MXene tribology. *Adv Mater* **35**(5): e2207757 (2023)

[29] Zhou X, Wang K L, Wu Y, Wang X B, Zhang X. Mussel-inspired interfacial modification for ultra-stable MoS_2 lubricating films with improved tribological behavior on nano-textured ZnO surfaces using the AACVD method. *ACS Appl Mater Interfaces* **14**(23): 27484–27494 (2022)

[30] Zhao Y, Mei H, Chang P, Yang Y B, Huang W F, Liu Y, Cheng L F, Zhang L T. 3D-printed topological MoS_2/$MoSe_2$ heterostructures for macroscale superlubricity. *ACS Appl Mater Interfaces* **13**(29): 34984–34995 (2021)

[31] Huang Q P, Shi X L, Xue Y W, Zhang K P, Gao Y Y, Wu C H. Synergetic effects of biomimetic microtexture with multi-solid lubricants to improve tribological properties of AISI 4140 steel. *Tribol Int* **167**: 107395 (2022)

[32] Lu C, Shi P Y, Yang J J, Jia J H, Xie E Q, Sun Y. Effects of surface texturing on the tribological behaviors of PEO/PTFE coating on aluminum alloy for heavy-load and long-performance applications. *J Mater Res Technol* **9**(6): 12149–12156 (2020)

[33] Wang B B, Lai W J, Li S J, Huang S T, Zhao X Y, You D Q, Tong X, Li W, Wang X J. Self-lubricating coating design strategy for titanium alloy by additive manufacturing. *Appl Surf Sci* **602**: 154333 (2022)

[34] Liu Y F, Li J J, Yi S, Ge X Y, Chen X C, Luo J B. Enhancement of friction performance of fluorinated graphene and molybdenum disulfide coating by microdimple arrays. *Carbon* **167**: 122–131 (2020)

[35] Vlădescu S C, Tadokoro C, Miyazaki M, Reddyhoff T, Nagamine T, Nakano K, Sasaki S, Tsujii Y. Exploiting the synergy between concentrated polymer brushes and laser surface texturing to achieve durable superlubricity. *ACS Appl Mater Interfaces* **14**(13): 15818–15829 (2022)

[36] Huang Q P, Wu C H, Shi X L, Xue Y W, Zhang K P. Synergistic lubrication mechanisms of AISI 4140 steel in dual lubrication systems of multi-solid coating and oil lubrication. *Tribol Int* **169**: 107484 (2022)

[37] Zhong Y H, Zheng L, Gao Y H, Liu Z N. Numerical simulation and experimental investigation of tribological performance on bionic hexagonal textured surface. *Tribol Int* **129**: 151–161 (2019)

[38] Chen P Y, Novitskaya E, Lopez M I, Sun C Y, McKittrick J. Toward a better understanding of mineral microstructure in bony tissues. *Bioinspired Biomim Nanobiomater* **3**(2): 71–84 (2014)

[39] Nazir A, Abate K M, Kumar A, Jeng J Y. A state-of-the-art review on types, design, optimization, and additive manufacturing of cellular structures. *Int J Adv Manuf Technol* **104**(9): 3489–3510 (2019)

[40] Huang N, Sang J B, Han K. A numerical simulation of the effects of snow particle shapes on blowing snow development. *J Geophys Res* **116**(D22): e2011jd016657 (2011)

[41] Hua X J, Sun J G, Zhang P Y, Liu K, Wang R, Ji J H, Fu Y H. Tribological properties of laser microtextured surface bonded with composite solid lubricant at high temperature. *J Tribol* **138**(3): 0313021–3130211 (2016)

[42] Zhan X, Liu Y, Yi P, Yin X, Fan C, Ma J. Parameter-dependent tribological properties of sinusoidal-textured plasma-sprayed coatings. *Tribology international* **174**: 107738 (2022)

[43] Lu G C, Lu W L, Shi X L, Zhai W Z, Zhang J, Yang Z J, Chen W G. Tribological properties and self-compensating lubrication mechanisms of Ni_3Al matrix bio-inspired shell-like composite structure. *Applied Surface Science* **573**: 151462 (2022).

[44] Hsu K C, Chen D H. Microwave-assisted green synthesis of Ag/reduced graphene oxide nanocomposite as a surface-enhanced Raman scattering substrate with high uniformity. *Nanoscale Res Lett* **9**(1): 193 (2014)

[45] Guo J, Chen J J, Lin Y Z, Liu Z M, Wang Y Q. Effects of surface texturing on nanotribological properties and subsurface damage of monocrystalline GaN subjected to scratching investigated using molecular dynamics simulation. *Appl Surf Sci* **539**: 148277 (2021)

Qipeng HUANG. He obtained his B.S. degree in process equipment and control engineering and M.S. degree in mechanical engineering from Henan University of Technology, Zhengzhou, China, in 2017 and 2020, respectively, and his Ph.D. degree in mechanical engineering from Wuhan University of Technology, Wuhan, China, in 2023. He is currently a post-doctoral fellow in traffic and transportation engineering at Wuhan University of Technology. His research interests focus on surface engineering, solid lubrication, design of functional materials, and tribology.

Chaohua WU. He received his B.S. degree in mechanical engineering and automation in 2003 from Wuhan University of Technology, Wuhan, China. He received his M.S. degree in mechanical manufacture and automation in 2006 from Wuhan University of Technology, Wuhan, China. He received his Ph.D. degree in industrial engineering from Wuhan University of Technology, Wuhan, China, in 2020. His current position is an assistant professor and a supervisor of graduates at the School of Mechanical and Electronic Engineering, Wuhan University of Technology. His research areas cover surface modification and process optimization.

Xiaoliang SHI. He received his B.S. degree in geological engineering in 1997 from China University of Geosciences, Wuhan, China. He received his M.S. and Ph.D. degrees in geological engineering from China University of Geosciences, Wuhan, China, in 2000 and 2003, respectively. His current position is a professor and a Ph.D. supervisor at the School of Mechanical and Electronic Engineering, Wuhan University of Technology, Wuhan, China. His research areas cover tribology and surface interface technology of high-end equipment.

Kaipeng ZHANG. He received his B.S. degree in industrial engineering in 2019 from Wuhan University of Technology, Wuhan, China. He is now a Ph.D. student in Wuhan University of Technology, Wuhan, China. His research areas cover textured surface, grease lubrication, and tribological properties of 2D materials tribology.